Confining sub-nanometer Pt clusters in hollow mesoporous carbon spheres for boosting hydrogen evolution activity

Wan, Xian-Kai; Wu, Hao Bin; Guan, Bu Yuan; Luan, Deyan; Lou, David Xiong Wen

2020

Wan, X.-K., Wu, H. B., Guan, B. Y., Luan, D., & Lou, D. X. W. (2020). Confining sub-nanometer Pt clusters in hollow mesoporous carbon spheres for boosting hydrogen evolution activity. Advanced Materials, 32(7), 1901349-. doi:10.1002/adma.201901349

https://hdl.handle.net/10356/138584

https://doi.org/10.1002/adma.201901349

Confining Subnanometer Pt Clusters in Hollow Mesoporous Carbon Spheres for Boosting Hydrogen Evolution Activity

*Xian-Kai Wan,[+] Hao Bin Wu,[+] Bu Yuan Guan, Deyan Luan, and Xiong Wen (David) Lou**

[*] Dr. X. K. Wan, Dr. B. Y. Guan, Dr. D. Y. Luan, Prof. X. W. Lou

School of Chemical and Biomedical Engineering, Nanyang Technological University, 62 Nanyang Drive, Singapore, 637459, (Singapore)

Email: xwlou@ntu.edu.sg; Webpage: http://www.ntu.edu.sg/home/xwlou/

Prof. H. B. Wu

School of Materials Science and Engineering, Zhejiang University, Hangzhou 310027, P. R. China

[+] X. K. Wan and H. B. Wu contributed equally to this work.

Abstract

Electrochemical water splitting has been considered as a promising approach to produce clean and sustainable hydrogen fuel. As a new class of nanomaterials with high ratio of surface atoms, tunable composition and electronic structure, metal clusters are promising candidates as catalysts. Here we demonstrate a new strategy to synthesize active and stable Pt-based electrocatalysts for hydrogen evolution by confining Pt clusters in hollow mesoporous carbon spheres (Pt_5/HMCS). Such a structure would effectively stabilize the Pt clusters during the ligand removal process, leading to remarkable electrocatalytic performance for hydrogen production in both acidic and alkaline solutions. Particularly, the optimal Pt_5/HMCS electrocatalyst exhibits 12 times the mass activity of Pt in commercial Pt/C catalyst with similar Pt loading. The present study exemplifies a simple yet effective approach to improve the cost-effectiveness of precious-metal-based catalysts with stabilized metal clusters.

Keywords: Pt clusters; mesoporous carbon; electrocatalysis; hydrogen evolution reaction

Hydrogen has been considered as an alternative green energy source to fossil fuels in view of its zero-pollution feature. Currently, hydrogen is mostly produced by natural gas reforming, which inevitably

leads to an increase of CO_2 emission. To realize a carbon neutral economy, producing hydrogen via electrocatalytic water splitting powered by electricity from renewable energy sources represents a feasible approach.[1-9] Despite the vast efforts devoted to develop efficient electrocatalysts for hydrogen evolution reaction (HER), Pt and Pt-based alloys remain the most active ones.[10-16] However, the high price and insufficient stability of Pt-based electrocatalysts limit their large-scale applications. Boosting the mass activity as well as the durability of Pt-based electrocatalysts becomes the key to reduce the cost of electrochemical hydrogen production. Conventional synthetic approaches for Pt-based electrocatalysts such as wet impregnation of metal salts followed by thermal reduction typically lead to large-size metal nanoparticles (NPs) with low atomic utilization. Moreover, precise modulation of active sites appears rather difficult due to the polydispersity of NPs.[17-22] Therefore, enhancing the catalytic activity and durability of Pt-based catalysts with atomic level precision remains a great challenge.

Metal clusters represent a new class of nanomaterials with well-defined chemical compositions and atomic structures, which are of particular interest in catalysis due to their high surface-to-volume ratio.[23-26] Compared with metal NPs, metal clusters display well-defined surface structure and abundant active sites for reactions that usually take place at surface/subsurface of catalysts, resulting in higher catalytic activity.[10, 27-33] However, detachment and agglomeration of clusters during operation would lead to severe degradation of performance, which limit their practical applications.[34] These drawbacks might be overcome by using catalyst supports with delicately designed nanostructure. For example, hollow mesoporous carbon spheres (HMCSs) would be attractive as catalyst supports comparing to conventional carbon supports.[35-38] Such a structure could provide large accessible surface to support clusters and facilitate ion/mass transport in the electrode. Additionally, the nanoscale pore channels might effectively confine clusters, thus to prevent the loss and agglomeration of clusters.

Herein, we demonstrate that efficient electrocatalysts for hydrogen production could be constructed by confining Pt-based clusters in nanostructured carbon hosts. As a proof of concept, $Pt_5(GS)_{10}$ clusters (GS = deprotonated glutathione) have been loaded into the pore channels of resorcinol formaldehyde (RF) derived HMCSs and subjected to ligand removal (**Figure 1**). The resulting composite electrocatalyst (denoted as Pt_5/HMCS) with ultrafine Pt clusters would in principle maximize the utilization of precious Pt atoms. Meanwhile, Pt clusters in nanopores exhibit enhanced stability and less tendency of agglomeration upon thermal treatment and during operation. As a result, remarkable electrocatalytic performance for HER in terms of activity and durability has been achieved in both acidic and alkaline solutions. In particular, the mass activity of the Pt_5/HMCS catalyst has been boosted by over one order of magnitude in alkaline solution compared to commercial Pt/C catalyst. Such a strategy for nanostructured electrocatalysts opens a new avenue to design and modulate cluster-based electrocatalysts at atomic level.

$Pt_5(GS)_{10}$ clusters were first synthesized according to a modified method (see Supporting Information for details).[39-41] The molecular purity of $Pt_5(GS)_{10}$ has been examined by UV-vis spectroscopy and matrix-assisted laser desorption ionization time-of-flight mass spectrometry (MALDI-TOF-MS).[42] The wide absorption band from 250 to 400 nm in the UV-vis spectrum is the fingerprint of $Pt_5(GS)_{10}$ clusters (Figure S1a, Supporting Information).[40] The MALDI mass spectrum of $Pt_5(GS)_{10}$ with a molecular ion peak at m/z = 4036 (**Figure 2**a) is in good agreement with the theoretical M_w of 4038 (with a deviation of 0.05 %). The characteristic patterns of vibrational stretching frequency in the Fourier transform-infrared (FT-IR) spectrum of $Pt_5(GS)_{10}$ (Figure S1b, Supporting Information) indicate the presence of ligands residing on the cluster surface. The peak corresponding to the S–H stretching vibration mode at 2526 cm^{-1} in the glutathione spectrum disappears in the spectrum of the $Pt_5(GS)_{10}$, evidencing the cleavage of S–H bond and binding of the ligand onto Pt atoms through Pt–S bonding. Thermogravimetric analysis (TGA) reveals that under air atmosphere the coordinating thiolate ligands start to decompose at about 200 °C and the content

of Pt (24.8 wt%) is close to the theoretical value (24.1 wt%) (Figure S1c, Supporting Information). Thus, $Pt_5(GS)_{10}$ clusters with a tiara-like structure, where Pt atoms bridged by thiol ligands rather than Pt-Pt interaction have been successfully synthesized (inset of Figure 2a).

A hard-template method has been adopted to fabricate HMCSs by carbonizing core–shell silica@silica/resorcinol formaldehyde (SiO_2@SiO_2/RF) nanospheres followed by removing the SiO_2 component (Figure 1, Step I).[35, 43] Field-emission scanning electron microscopy (FESEM) and transmission electron microscopy (TEM) images confirm the uniformity of the as-prepared SiO_2@SiO_2/C nanospheres with a core-shell structure of around 240 nm in diameter (Figure S2a and b, Supporting Information). Selectively etching away SiO_2 gives a well-define hollow structure with mesoporous shell and radially aligned pore channels (Figure S2c, Supporting Information). Such a nanoporous architecture results in a high Brunauer–Emmett–Teller (BET) surface area and a large pore volume of 1534 m^2g^{-1} and 2.14 cm^3g^{-1} (Figure S3a, Supporting Information), respectively. Uniform pore channels of 5.2 nm estimated by BJH method would easily accommodate NCs while warranting sufficient mass transport (Figure S3b, Supporting Information).

To incorporate $Pt_5(GS)_{10}$ clusters into HMCSs, an aqueous solution containing $Pt_5(GS)_{10}$ clusters and HMCSs has been vigorously stirred for 10 h and then completely dried under decompression condition at 60 °C for 12 h (Figure 1, Step II). The $Pt_5(GS)_{10}$/HMCS nanocomposite well preserves the pristine morphology of HMCS host (Figure S4, Supporting Information). TEM observation on the composite particles as shown in Figure 2b reveals a similar texture compared to HMCS due to the low contrast of $Pt_5(GS)_{10}$ clusters and the absence of aggregation. Nevertheless, the uniform loading of $Pt_5(GS)_{10}$ clusters into the porous matrix is verified by the high-resolution TEM (HRTEM) image (Figure 2c), where dark dots with size less than 1 nm correspond to the monodisperse $Pt_5(GS)_{10}$ clusters.

X-ray photoelectron spectroscopy (XPS) spectrum of $Pt_5(GS)_{10}$ clusters confirms the presence of Pt element in the form of Pt^{2+} (Figure S5a, Supporting Information), which is consistent with the

proposed structure. Two peaks with binding energies of 72.5 and 75.8 eV correspond to the Pt $4f_{7/2}$ and Pt $4f_{5/2}$ of Pt^{2+}, respectively. Such Pt^{2+} species in the $Pt_5(GS)_{10}$ clusters could be adopted to selectively produce zero-valent Pt under hydrogen gas stream and appropriate calcination condition (Figure 1, Step III).[41, 44] The thermal stability of the $Pt_5(GS)_{10}$ clusters was investigated by thermogravimetric analysis (TGA) to establish appropriate calcination conditions (Figure S5b, Supporting Information). In a non-oxidative environment, elimination of the coordinating thiolate ligands begins at around 200 °C, whereas complete removal of ligands is not achieved even up to 700 °C. Thus, a compromise between ligand removal and agglomeration of nanoclusters at elevated temperature should be made. To determine the optimal calcination condition, $Pt_5(GS)_{10}$/HMCS is treated at different temperature in a mixed H_2/Ar (5 % H_2) gas flow to obtain a Pt_5/HMCS electrocatalyst with a Pt loading of 5.08 wt%. The electrocatalytic activity of various Pt_5/HMCS samples is probed by HER in alkaline condition (1.0 M KOH), the kinetics of which is more sluggish compared with that in acidic condition. The best performing electrocatalyst is achieved with a moderate annealing temperature of 550 ºC for 15 h (Figure S6, Supporting Information). Meanwhile, increasing the loading of Pt clusters in the composite electrocatalysts enhances the activity until reaching an optimal value of 5.08 wt%. Further increase of Pt loading does not favor the HER in both acidic and alkaline conditions (Figure S7, Supporting Information).

The effect of annealing temperature is first revealed by x-ray diffraction (XRD) analysis (Figure S8a, Supporting Information). Distinct diffraction peaks of (111) and (200) planes of Pt observed with temperature over 650 °C indicate severe agglomeration of Pt clusters into larger NPs with long-range order. Further increasing the loading of Pt clusters would also promote the agglomeration due to shorter distance between $Pt_5(GS)_{10}$ clusters (Figure S8b, Supporting Information), which is consistent with the inferior performance of Pt_5/HMCS electrocatalysts with Pt loading higher than 5.08 wt%.[45] The monodisperse and discrete Pt clusters on HMCSs in the optimal sample (Pt_5/HMCS-5.08%) are directly observed by high-angle annular dark-field scanning transmission

electron microscopy (HAADF-STEM) observation. Pt clusters appearing as bright dots in the dark-field image are well dispersed on the porous carbon supports (**Figure 3**a). Majority of the Pt clusters remains in sub-nanometer (~ 0.77 nm) size (Figure 3b), which are presumably assembly of a few Pt atoms after removing the ligands from $Pt_5(GS)_{10}$ clusters and verified by the magnified HAADF-STEM image with atomic resolution (Figure 3b inset). As shown in Figure 3c, elemental mapping of a single particle of Pt_5/HMCS-5.08% reveals a uniform distribution of Pt species within the mesoporous carbon shell. In addition, minor signal from sulfur is detected, which suggests the presence of residual ligands.

The Pt clusters on HMCS after ligand removal at different temperatures are further characterized by x-ray energy dispersive spectroscopy (EDS) as shown in **Figure 3**d. The content of S notably decreases upon thermal treatment, as the molar ratio of Pt:S increases from 0.5 in pristine $Pt_5(GS)_{10}$ clusters to about 5 after annealing at 650 ^oC. The incomplete removal of S-containing ligands at such temperature is also consistent with the TGA result as discussed earlier. XPS is further used to get insight of the electronic structure (Figure 3e). As the annealing temperature increases, the binding energy of Pt $4f_{7/2}$ moves towards lower binding energy. Deconvolution of the spectrum gives a new peak with a binding energy of 71.6 eV, which is in line with the reported Pt_{12} clusters produced by dendrimer-reactor and $[Pt(\mu\text{-}SC_8H_{17})_2]_{12}$.[41, 44] Thus, increasing the annealing temperature simultaneously eliminates thiol ligands and reduces Pt^{2+} to metallic Pt^0. With a relatively low annealing temperature of 350 °C, about 2/3 of Pt still exists as Pt^{2+}, explaining its inferior electrocatalytic activity. Further raising the temperature to 550 °C converts about 3/4 of Pt to metallic Pt^0 in the optimal Pt_5/HMCS sample, offering sufficient active sites for hydrogen evolution. In addition, the co-existence of Pt^0 and Pt^{2+} in Pt clusters results in an electronic structure distinctly different from common NPs, which might lead to higher intrinsic catalytic activity.

To illustrate the possible advantages of our synthetic approach, control experiments have been done to synthesize Pt-based electrocatalysts by replacing $Pt_5(GS)_{10}$ with H_2PtCl_6 and HMCS with

carbon black (CB) while other conditions remain unaltered. The resulting electrocatalysts with identical Pt content are denoted as Pt_{Cl}/HMCS-5.08% and Pt_5/CB-5.08%, respectively. XRD pattern of Pt_{Cl}/HMCS-5.08% with sharp diffraction peaks of metallic Pt suggests relatively large NPs (Figure 3f). As confirmed by TEM and HAADF-STM images (Figure S9, Supporting Information), Pt synthesized by direct reduction of inorganic salt tends to form relatively large NPs with polydispersity even in the mesoporous channels with physical barrier. Meanwhile, $Pt_5(GS)_{10}$ clusters annealed and reduced on CB support result in minor diffraction peaks in the XRD pattern. Thus, minor agglomeration of Pt clusters occurs on conventional high-surface-area carbon supports (Figure S10, Supporting Information), verifying the superiority of Pt clusters confined in the mesoporous channels of HMCSs. To further reveal the role of mesoporous channels, HMCSs with different pore sizes were synthesized and employed as the supports for $Pt_5(GS)_{10}$ clusters. By varying the synthetic parameters, the average pore size of HMCSs could be tuned from 2 to 10 nm (Figure S11, Supporting Information). After the identical procedure to incorporate $Pt_5(GS)_{10}$ clusters and to remove ligands, partial agglomeration of Pt clusters occurs in HMCSs with small (2 nm) mesopores and the situation is worse with large (10 nm) mesopores (Figure S12, Supporting Information). The difficulty of infiltrating $Pt_5(GS)_{10}$ clusters into small mesopores and the less sterical hindrance in large mesopores would explain the optimal confinement of clusters in HMCSs with moderate pore size (i.e., 5 nm). Thus, both the suitable pore structure of the HMCSs host and the in-situ ligand removal of pre-synthesized clusters in the nanochannels are responsible for the formation of sub-nanometer Pt catalysts, which is significantly different from previous reports of nanoparticles confined in porous carbon hosts.[46, 47]

Electrocatalytic activity of the Pt_5/HMCS catalyst for HER was examined in both acidic (0.5 M H_2SO_4) and alkaline (1.0 M KOH) aqueous solutions using a typical three-electrode setup. We first calibrated the Ag/AgCl (KCl saturated) reference electrode against a reversible hydrogen electrode (RHE) constructed with a Pt wire and a Pt sheet in 0.5 M H_2SO_4 and 1.0 M KOH saturated with H_2

(Figure S13, Supporting Information). Commercial Pt/C catalysts (Pt loadings of 5 and 20 wt%, denoted as Pt/C-5% and Pt/C-20%, respectively) have also been tested for comparison. The *iR*-compensated polarization curves (current density is normalized by geometric area of the electrode) recorded in acidic and alkaline solutions are shown in **Figure 4**a and b, respectively. The poor HER activity of Pt-free HMCS as the blank control verifies that the high electrocatalytic activity of the Pt_5/HMCS catalyst indeed originates from the Pt clusters. Notably, the activity of the Pt_5/HMCS catalyst for HER is higher than that of commercial Pt/C-5% catalysts with similar Pt content especially in alkaline solution, and close to that of Pt/C-20% with 4 times of Pt loading. Only small overpotentials of 20.7 and 46.2 mV are required to drive a current density of 10 mA cm^{-2} for hydrogen production in acidic and alkaline solutions, respectively. Thus, much higher utilization of Pt moieties is expected in the form of clusters compared to conventional NPs. The mass activity of Pt in the commercial Pt/C and Pt_5/HMCS catalysts is further compared. In acidic condition, the mass activity gradually decreases as the Pt content increases in Pt_5/HMCS catalysts at -30 mV (vs. RHE) (Figure 4c), probably due to mass transport limit and/or agglomeration of Pt clusters. In alkaline condition, however, the maximal mass activity is achieved with Pt_5/HMCS-5.08% at -70 mV (vs. RHE) (Figure 4d). In all cases, the mass activity of Pt_5/HMCS catalysts is notably higher than that of commercial Pt/C. For example, for the relatively sluggish HER in alkaline solution, the Pt_5/HMCS-5.08% sample presents a mass activity of 3.23 mA μg^{-1}_{Pt}, which is 4.96 and 12.42 times of that of the commercial Pt/C-20% (0.65 mA μg^{-1}_{Pt}) and Pt/C-5% (0.26 mA μg^{-1}_{Pt}), respectively. Comparing with the state-of-the-art Pt-based or single-atom-based electrocatalysts, our Pt_5/HMCS catalysts exhibit very attractive electrocatalytic activity for HER in both acidic and alkaline condition (Table S1 and S2, Supporting Information). Considering the absence of co-catalyst of the Pt_5/HMCS catalysts, further enhancement of electrocatalytic performance is highly anticipated.

Electrochemical impedance spectroscopy (EIS) is employed to analyze the different electrocatalytic activity of Pt_5/HMCS and Pt/C. Consistent with previous studies, the Nyquist plots

of Pt_5/HMCS in both acidic and basic solutions exhibit two semicircles (Figure S14, Supporting Information). The first one at high frequency is related to the surface porosity of the electrode, while the second one at low frequency, which depends on the overpotential, reflects the charge transfer process during HER.[8, 48] As shown in Figure S15 (Supporting Information), the charge-transfer resistance (R_{ct}) is strongly correlated with the electrocatalytic activity. Pt_5/HMCS shows much smaller R_{ct} than Pt/C under the same overpotential especially in basic condition, which explains the higher HER activity of Pt_5/HMCS. The gaseous products from the Pt_5/HMCS-5.08% electrode is quantified by gas chromatography. Only H_2 is detected and the amount of measured H_2 matches well with the calculated result (Figure S16, Supporting Information), indicating a nearly 100% Faradaic efficiency.

To assess the durability of the Pt_5/HMCS-5.08% electrocatalyst, accelerated cyclic voltammetry was conducted repeatedly on the electrodes at a scan rate of 50 mV s^{-1} (Figure 4e and f). In both acidic and alkaline conditions, the polarization curves show a small shift of around 3 mV at j =10 mA cm^{-2} after 3,000 sweeps. In a sharp contrast, the commercial Pt/C-5% catalyst experiences significant degradation with obvious increase in overpotential (18 mV in acidic solution and 64 mV in alkaline solution) after the same measurement. The Pt_5/HMCS-5.08% after durability test was subjected to TEM analysis. After testing in acidic solution, the catalyst remains intact without agglomeration of Pt clusters (Figure S17, Supporting Information). On the contrary, there is some slight increase in the size of Pt clusters in alkaline solution, possibly due to minor corrosion of HMCS support (Figure S18, Supporting Information). The stability of catalysts is also evaluated under constant current condition as shown by the *i-t* curves of Pt_5/HMCS-5.08% and commercial Pt/C-20% (Figure S19, Supporting Information), which against verify the improved stability of Pt_5/HMCS-5.08% in both acidic and alkaline conditions. Nevertheless, Pt clusters residing in the mesopore channels of HMCSs have been effectively stabilized, leading to exceptionally high activity and durability.

To understand the structural advantages of the Pt_5/HMCS catalysts, Pt_5/HMCS-5.08% is compared with Pt_{Cl}/HMCS-5.08% and Pt_5/CB-5.08% with the same Pt content (**Figure 5**a and b). Pt_{Cl}/HMCS-5.08% exhibits the worse electrocatalytic activity, likely due to the severe merge of Pt moieties into relatively large NPs. These Pt NPs in Pt_{Cl}/HMCS-5.08% differ from Pt clusters in Pt_5/HMCS-5.08% in terms of size, morphology and electronic structure.[19, 23, 49] Minor agglomeration of Pt clusters also leads to inferior electrocatalytic activity. In addition, comparing the HER activities of Pt_5/HMCS catalysts with different pore sizes, the sample with mesopores of 5 nm in size exhibits the optimal performance (Figure S20, Supporting Information), which is in accordance with their structural feature. For Pt_5/HMCS with small mesopores, poor electrolyte contact and mass transport limit might be the major causes for the inferior activity. For Pt_5/HMCS with large mesopores, the notably increased size of Pt clusters could account for the degraded activity. The above results signify the high catalytic activity of Pt clusters and the importance to confine the Pt clusters into nanoporous channels with suitable size.

Intuitively one would expect the remarkable performance of Pt clusters originates from the high surface area with dominant surface Pt atoms. Thus, the apparent electrochemical surface areas (ECSAs) of Pt_5/HMCS-5.08% and commercial Pt/C catalysts are measured by a CO stripping method (Figure S21, Supporting Information) to quantify the surface effect of Pt clusters.[50-52] Surprisingly, the ECSAs of these three catalysts lie in the order of Pt/C-20% < Pt_5/HMCS-5.08% < Pt/C-5%. The ECSA of Pt_5/HMCS-5.08% is below the expectation for such ultra-small clusters, which might be due to the incomplete removal of ligands as discussed earlier. Normalizing the HER current to the ECSAs of Pt components gives the intrinsic activity of accessible surface Pt atoms. As shown in **Figure** 5c and d, with identical ECSA of Pt, Pt_5/HMCS-5.08% exhibits overwhelming advantage over commercial Pt/C catalysts especially in alkaline solution. The turnover frequencies (TOFs) could be estimated by assuming all Pt atoms are active (Figure S22, Supporting Information). In alkaline solution, the TOF of Pt_5/HMCS-5.08% at an overpotential of 100 mV is 8.8 s^{-1}, which is about 5.6

and 15.2 times higher than that of Pt/C-20% and Pt/C-5%. Compared with other benchmark electrocatalysts in similar condition, the TOF of the Pt_5/HMCS-5.08% catalyst is 11, 2200 and 176 times higher than those of Ni_5P_4 (0.8 s^{-1}),[53] Ni_2P (0.004 s^{-1}),[53] and Ni-Mo alloy (0.05 s^{-1}),[7] respectively. In addition, we evaluate the HER activity of the Pt-based catalysts loaded on carbon fiber paper (CFP) at relatively large overpotential to assess their performance in a more realistic situation. As shown in Figure S23 (Supporting Information), in high-current-density region (close to 100 mA cm^{-2}), Pt_5/HMCS catalyst maintains the best catalytic activity in both acidic and alkaline solutions, suggesting its superiority in practical applications. We envision that the high catalytic performance does not only come from the high surface area of Pt clusters, which might be also related to the special atomic/electronic structure and enhanced mass transport of the sub-nanometer Pt clusters well supported on HMCSs.

We further evaluated the Tafel plots to give mechanistic insights into the outstanding catalytic activity of Pt_5/HMCS-5.08% for HER. Although a previous study pointed out that deriving Tafel slope and exchange current density from experimental data would be interfered by mass transport limitation,[54] comparing the apparent "Tafel slope" at relatively small overpotential would still provide some mechanistic information of the electrocatalysts. In both acidic (Figure 5e) and alkaline (Figure 5f) conditions, the commercial Pt/C-20% catalyst with a higher Pt loading exhibits higher reaction kinetics with lower Tafel slope than those of Pt/C-5% (28.4 mV dec^{-1} vs. 40.2 mV dec^{-1} in acidic electrolyte and 56.6 mV dec^{-1} vs. 182.3 mV dec^{-1} in basic electrolyte), highlighting the sensitivity of electrocatalytic mechanism to the atomic and nanostructure of catalysts. Pt_5/HMCS-5.08% shows small Tafel slopes of 28.3 mV dec^{-1} and 48.1 mV dec^{-1} in acidic and alkaline conditions, respectively, which are even superior to the Pt/C-20% catalyst. Meanwhile, the control electrocatalyst of Pt NPs supported on HMCS (Pt_{Cl}/HMCS-5.08%), which possesses similar pore structure and thus similar mass transport behavior, only exhibits moderate Tafel slopes. Therefore, the fast hydrogen evolution kinetics could be ascribed to the discrete Pt clusters within easily accessible pore channels.

In particular, the advantage of Pt_5/HMCS-5.08% is more pronounced in alkaline electrolyte, which might be related to the accelerated water dissociation on Pt clusters.

In summary, we report an effective strategy to construct active and durable electrocatalysts for hydrogen evolution by confining Pt clusters in hollow mesoporous carbon spheres (Pt_5/HMCS). The use of ultra-small clusters would in principle maximize the utilization of the precious Pt atoms while offer distinct surface and electronic structure compared with conventional Pt nanoparticles. Immobilizing the Pt clusters in the mesoporous channels of carbon support would effectively stabilize the highly active Pt clusters during ligand removal and electrochemical hydrogen production. The electrocatalytic activity of the optimal Pt_5/HMCS electrocatalyst with a relatively low Pt loading of 5.08 wt% would exceed that of commercial Pt/C with a much higher Pt loading of 20 wt%, thus offering much higher mass activity of Pt. Particularly, in alkaline electrolyte where Pt usually exhibits inferior performance, the mass activity of Pt_5/HMCS would be over 12 times that of commercial Pt/C with similar Pt loading. Together with the ameliorated durability, the cost-effectiveness of electrochemical hydrogen evolution could be much improved with the Pt_5/HMCS electrocatalysts developed here. Using atomically precious clusters to construct catalytic sites might also be applicable to other systems even for earth-abundant catalysts. Thus, we hope that this work would shed some light on the designed synthesis of high-performance catalysts with delicately controlled active centers.

Acknowledgements

X. W. Lou acknowledges the funding support from the National Research Foundation (NRF) of Singapore via the NRF investigatorship (NRF-NRFI2016-04). We thank Profs. Satoshi Muratsugu and Mizuki Tada from Nagoya University for kind support in some TEM characterization during revision.

References

[1] R. Subbaraman, D. Tripkovic, D. Strmcnik, K.-C. Chang, M. Uchimura, A. P. Paulikas, V. Stamenkovic, N. M. Markovic, *Science* **2011**, *334*, 1256.

[2] J. A. Turner, *Science* **2004**, *305*, 972.

[3] M. G. Walter, E. L. Warren, J. R. McKone, S. W. Boettcher, Q. Mi, E. A. Santori, N. S. Lewis, *Chem. Rev.* **2010**, *110*, 6446.

[4] T. R. Cook, D. K. Dogutan, S. Y. Reece, Y. Surendranath, T. S. Teets, D. G. Nocera, *Chem. Rev.* **2010**, *110*, 6474.

[5] M. Cabán-Acevedo, M. L. Stone, J. R. Schmidt, J. G. Thomas, Q. Ding, H.-C. Chang, M.-L. Tsai, J.-H. He, S. Jin, *Nat. Mater.* **2015**, *14*, 1245.

[6] Y. Jiao, Y. Zheng, K. Davey, S.-Z. Qiao, *Nat. Energy* **2016**, *1*, 16130.

[7] E. J. Popczun, J. R. McKone, C. G. Read, A. J. Biacchi, A. M. Wiltrout, N. S. Lewis, R. E. Schaak, *J. Am. Chem. Soc.* **2013**, *135*, 9267.

[8] H. B. Wu, B. Y. Xia, L. Yu, X.-Y. Yu, X. W. Lou, *Nat. Commun* **2015**, *6*, 6512.

[9] D. Voiry, H. Yamaguchi, J. Li, R. Silva, D. C. B. Alves, T. Fujita, M. Chen, T. Asefa, V. B. Shenoy, G. Eda, M. Chhowalla, *Nat. Mater.* **2013**, *12*, 850.

[10] J. N. Tiwari, S. Sultan, C. W. Myung, T. Yoon, N. Li, M. Ha, A. M. Harzandi, H. J. Park, D. Y. Kim, S. S. Chandrasekaran, W. G. Lee, V. Vij, H. Kang, T. J. Shin, H. S. Shin, G. Lee, Z. Lee, K. S. Kim, *Nat. Energy* **2018**, *3*, 773.

[11] H. Yin, S. Zhao, K. Zhao, A. Muqsit, H. Tang, L. Chang, H. Zhao, Y. Gao, Z. Tang, *Nat. Commun* **2015**, *6*, 6430.

[12] Z. Cao, Q. Chen, J. Zhang, H. Li, Y. Jiang, S. Shen, G. Fu, B.-a. Lu, Z. Xie, L. Zheng, *Nat. Commun* **2017**, *8*, 15131.

[13] Z. Zhao, H. Liu, W. Gao, W. Xue, Z. Liu, J. Huang, X. Pan, Y. Huang, *J. Am. Chem. Soc.* **2018**, *140*, 9046.

[14] H. Zhang, P. An, W. Zhou, B. Y. Guan, P. Zhang, J. Dong, X. W. Lou, *Sci. Adv.* **2018**, *4*, eaao6657.

[15] P. Wang, K. Jiang, G. Wang, J. Yao, X. Huang, *Angew. Chem. Int. Ed.* **2016**, *55*, 12859.

[16] P. Wang, X. Zhang, J. Zhang, S. Wan, S. Guo, G. Lu, J. Yao, X. Huang, *Nat. Commun* **2017**, *8*, 14580.

[17] L. Liu, A. Corma, *Chem. Rev.* **2018**, *118*, 4981.

[18] J. Feng, Y. He, Y. Liu, Y. Du, D. Li, *Chem. Soc. Rev.* **2015**, *44*, 5291.

[19] L. Guo, W.-J. Jiang, Y. Zhang, J.-S. Hu, Z.-D. Wei, L.-J. Wan, *ACS Catal.* **2015**, *5*, 2903.

[20] B. Jiang, C. Li, V. Malgras, M. Imura, S. Tominaka, Y. Yamauchi, *Chem. Sci.* **2016**, *7*, 1575.

[21] C. Li, H. Tan, J. Lin, X. Luo, S. Wang, J. You, Y.-M. Kang, Y. Bando, Y. Yamauchi, J. Kim, *Nano Today* **2018**, *21*, 91.

[22] C. Li, M. Iqbal, J. Lin, X. Luo, B. Jiang, V. Malgras, K. C. W. Wu, J. Kim, Y. Yamauchi, *Acc. Chem. Res.* **2018**, *51*, 1764.

[23] R. Jin, C. Zeng, M. Zhou, Y. Chen, *Chem. Rev.* **2016**, *116*, 10346.

[24] K. Kwak, W. Choi, Q. Tang, M. Kim, Y. Lee, D.-e. Jiang, D. Lee, *Nat. Commun* **2017**, *8*, 14723.

[25] S. Zhao, R. Jin, H. Abroshan, C. Zeng, H. Zhang, S. D. House, E. Gottlieb, H. J. Kim, J. C. Yang, R. Jin, *J. Am. Chem. Soc.* **2017**, *139*, 1077.

[26] I. Chakraborty, T. Pradeep, *Chem. Rev.* **2017**, *117*, 8208.

[27] E. C. Tyo, S. Vajda, *Nature. Nanotechnol.* **2015**, *10*, 577.

[28] M. Boronat, A. Leyva-Pérez, A. Corma, *Acc. Chem. Res.* **2014**, *47*, 834.

[29] S. Yamazoe, K. Koyasu, T. Tsukuda, *Acc. Chem. Res.* **2014**, *47*, 816.

[30] W. Zhong‐Li, S. Keju, H. Joel, H. Xianfeng, L. Cuiling, T. Toshiaki, K. Yong‐Mook, Y. Yusuke, *Angew. Chem. Int. Ed.* **2018**, *57*, 5848.

[31] A. von Weber, S. L. Anderson, *Acc. Chem. Res.* **2016**, *49*, 2632.

[32] X.-K. Wan, J.-Q. Wang, Z.-A. Nan, Q.-M. Wang, *Sci. Adv.* **2017**, *3*, e1701823.

[33] Y. Wang, X.-K. Wan, L. Ren, H. Su, G. Li, S. Malola, S. Lin, Z. Tang, H. Häkkinen, B. K. Teo, Q.-M. Wang, N. Zheng, *J. Am. Chem. Soc.* **2016**, *138*, 3278.

[34] L. Liu, U. Díaz, R. Arenal, G. Agostini, P. Concepción, A. Corma, *Nat. Mater.* **2016**, *16*, 132.

[35] H. Zhang, O. Noonan, X. Huang, Y. Yang, C. Xu, L. Zhou, C. Yu, *ACS Nano* **2016**, *10*, 4579.

[36] D.-S. Yang, D. Bhattacharjya, S. Inamdar, J. Park, J.-S. Yu, *J. Am. Chem. Soc.* **2012**, *134*, 16127.

[37] T. Yang, H. Ling, J.-F. Lamonier, M. Jaroniec, J. Huang, M. J. Monteiro, J. Liu, *NPG. Asia. Mater.* **2016**, *8*, e240.

[38] J. Liu, N. P. Wickramaratne, S. Z. Qiao, M. Jaroniec, *Nat. Mater.* **2015**, *14*, 763.

[39] K. Yamamoto, T. Imaoka, W. J. Chun, O. Enoki, H. Katoh, M. Takenaga, A. Sonoi, *Nat Chem* **2009**, *1*, 397.

[40] A. George, K. S. Asha, A. C. Reber, S. R. Biltek, A. F. Pedicini, A. Sen, S. N. Khanna, S. Mandal, *Nanoscale* **2015**, *7*, 19448.

[41] T. Imaoka, Y. Akanuma, N. Haruta, S. Tsuchiya, K. Ishihara, T. Okayasu, W.-J. Chun, M. Takahashi, K. Yamamoto, *Nat. Commun* **2017**, *8*, 688.

[42] X.-K. Wan, Z.-J. Guan, Q.-M. Wang, *Angew. Chem. Int. Ed.* **2017**, *56*, 11494.

[43] Z. Li, J. Zhang, B. Y. Guan, X. W. D. Lou, *Angew. Chem. Int. Ed.* **2017**, *56*, 16003.

[44] T. Imaoka, H. Kitazawa, W.-J. Chun, S. Omura, K. Albrecht, K. Yamamoto, *J. Am. Chem. Soc.* **2013**, *135*, 13089.

[45] T. Yoskamtorn, S. Yamazoe, R. Takahata, J.-i. Nishigaki, A. Thivasasith, J. Limtrakul, T. Tsukuda, *ACS Catal.* **2014**, 3696.

[46] C. Galeano, J. C. Meier, V. Peinecke, H. Bongard, I. Katsounaros, A. A. Topalov, A. Lu, K. J. J. Mayrhofer, F. Schüth, *J. Am. Chem. Soc.* **2012**, *134*, 20457.

[47] S. Mezzavilla, C. Baldizzone, K. J. J. Mayrhofer, F. Schüth, *ACS Appl. Mater.Interfaces* **2015**, *7*, 12914.

[48] L. Liao, S. Wang, J. Xiao, X. Bian, Y. Zhang, M. D. Scanlon, X. Hu, Y. Tang, B. Liu, H. H. Girault, *Energy Environ. Sci.* **2014**, *7*, 387.

[49] K. An, S. Alayoglu, N. Musselwhite, K. Na, G. A. Somorjai, *J. Am. Chem. Soc.* **2014**, *136*, 6830.

[50] W. Sheng, H. A. Gasteiger, Y. Shao-Horn, *J. Electrochem. Soc.* **2010**, *157*, B1529.

[51] A. Pozio, M. De Francesco, A. Cemmi, F. Cardellini, L. Giorgi, *J. Power Sources* **2002**, *105*, 13.

[52] H. Xu, A.-L. Wang, Y.-X. Tong, G.-R. Li, *ACS Catal.* **2016**, *6*, 5198.

[53] A. B. Laursen, K. R. Patraju, M. J. Whitaker, M. Retuerto, T. Sarkar, N. Yao, K. V. Ramanujachary, M. Greenblatt, G. C. Dismukes, *Energy Environ. Sci.* **2015**, *8*, 1027.

[54] A. R. Kucernak, C. Zalitis, *J. Phys. Chem. C* **2016**, *120*, 10721.

Figures and captions

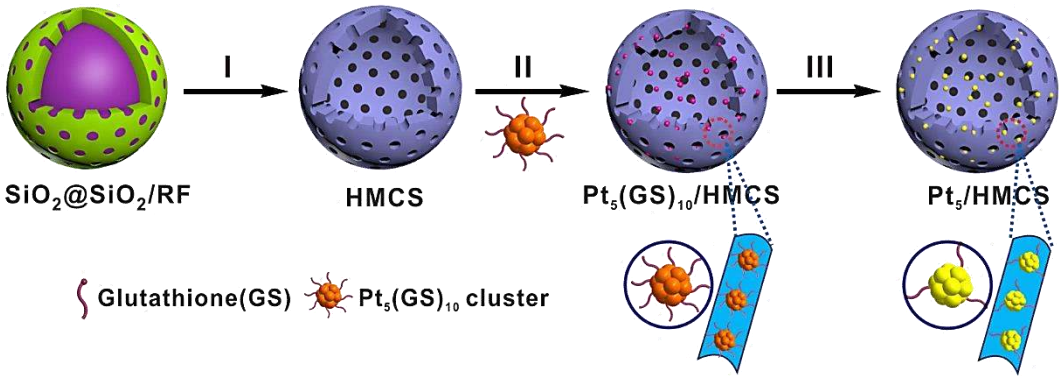

Figure 1. Schematic illustration of the synthetic procedure of Pt_5/HMCS. Step I: carbonization and etching of SiO_2 to form HMCS. Step II: loading the $Pt_5(GS)_{10}$ clusters onto HMCS to form $Pt_5(GS)_{10}$/HMCS. Step III: conversion of $Pt_5(GS)_{10}$/HMCS to Pt_5/HMCS electrocatalyst through thermal treatment.

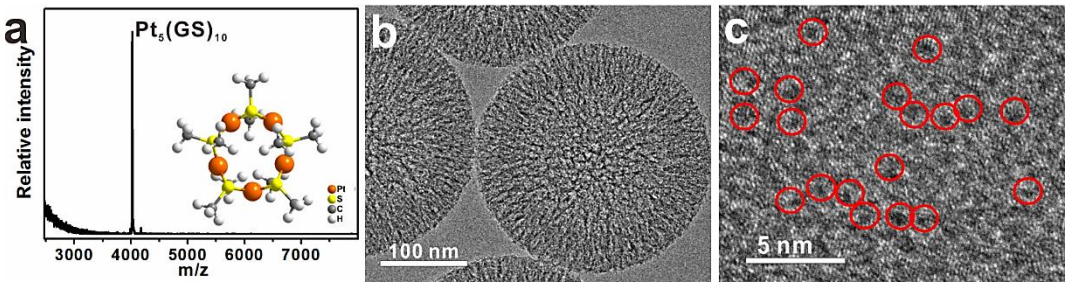

Figure 2. Characterizations of $Pt_5(GS)_{10}$ clusters and $Pt_5(GS)_{10}$/HMCS. (a) MALDI-TOF-MS characterization of the $Pt_5(GS)_{10}$ clusters; inset: the structure of a $Pt_5(GS)_{10}$ cluster (the GS is glutathione and replaced by SCH_3 for clarity). (b) TEM and (c) HRTEM images of $Pt_5(GS)_{10}$/HMCS.

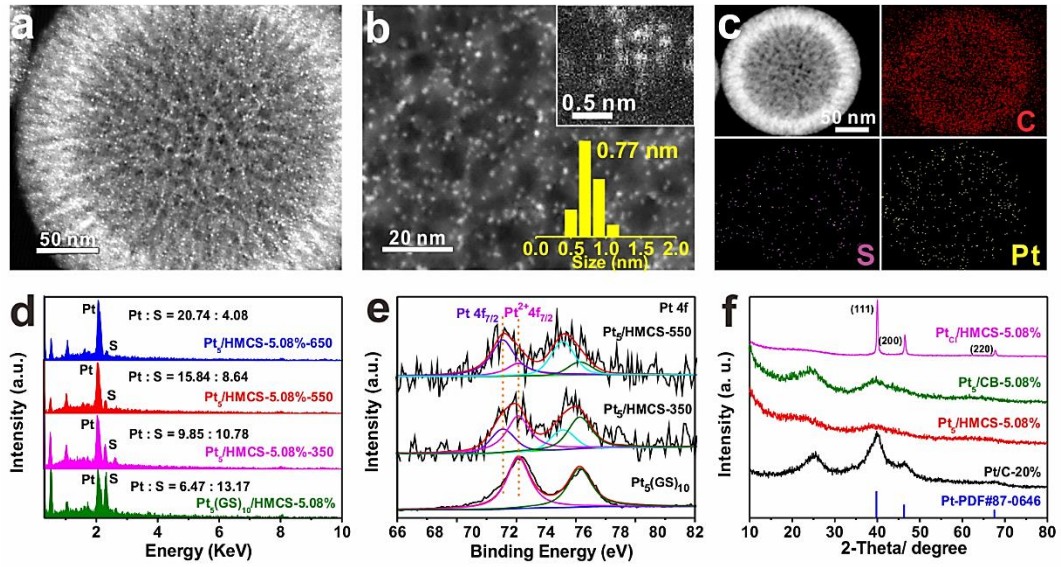

Figure 3. Materials characterizations of the Pt_5/HMCS electrocatalyst. (a, b) HAADF-STEM images (inset: size distribution of the Pt clusters and magnified image of Pt cluster) and (c) elements mapping of $Pt_5(GS)_{10}$/HMCS after thermal treatment. (d) EDX of $Pt_5(GS)_{10}$/HMCS-5.08% with different annealing temperatures. (e) Pt 4f XPS spectra comparison of $Pt_5(GS)_{10}$ and $Pt_5(GS)_{10}$/HMCS-5.08% with different annealing temperatures. (f) XRD patterns of standard Pt (PDF # 87-0646), Pt_5/HMCS-5.08%, Pt_5/CB-5.08%, Pt_{Cl}/HMCS-5.08% and commercial Pt/C-20%).

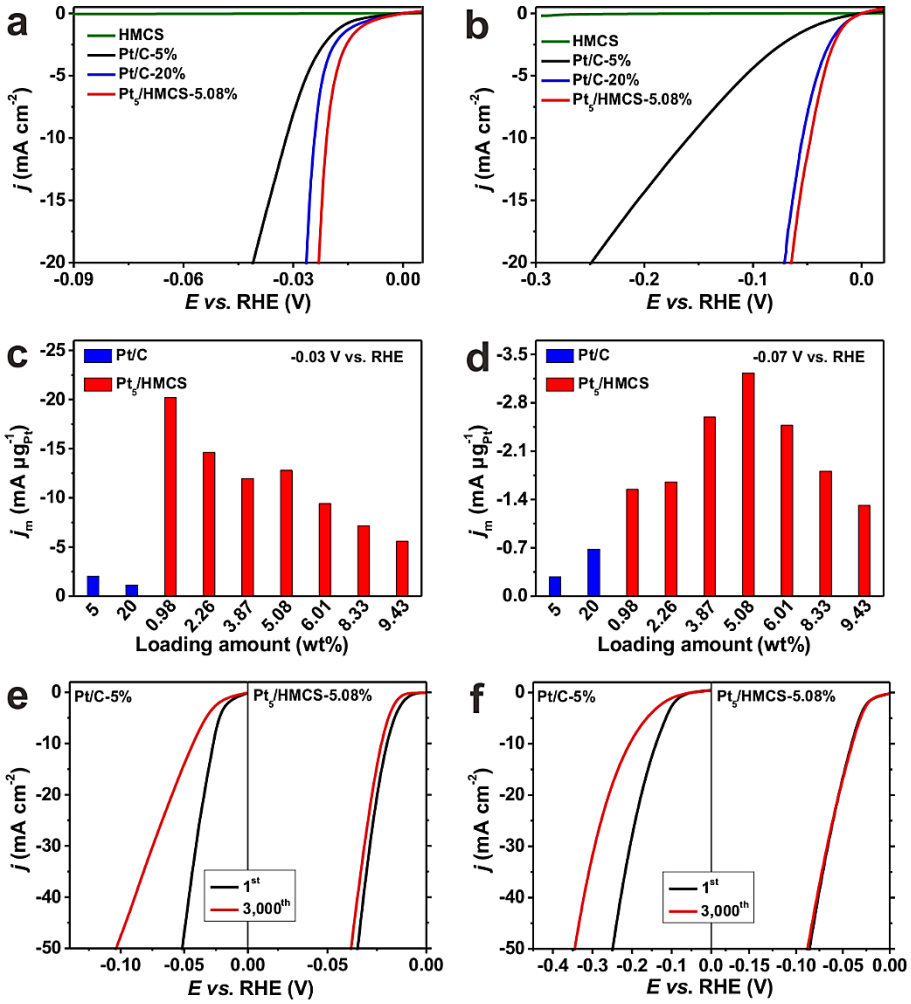

Figure 4. Electrocatalytic hydrogen evolution using Pt_5/HMCS electrocatalyst. LSV curves of Pt_5/HMCS-5.08% and commercial Pt/C (5 wt% and 20 wt%) catalysts based on geometric area of the working electrode in (a) 0.5 M H_2SO_4 and (b) 1.0 M KOH. Mass activities of commercial Pt/C and Pt_5/HMCS catalysts with different Pt loadings (c) at an overpotential of 0.03 V (vs. RHE) in 0.5 M H_2SO_4 and (d) at an overpotential of 0.07 V (vs. RHE) in 1.0 M KOH. Polarization curves of Pt/C-5% (left) and Pt_5/HMCS-5.08% (right) after continuous potential sweeps at 50 mV s^{-1} in (e) 0.5 M H_2SO_4 and (f) 1.0 M KOH.

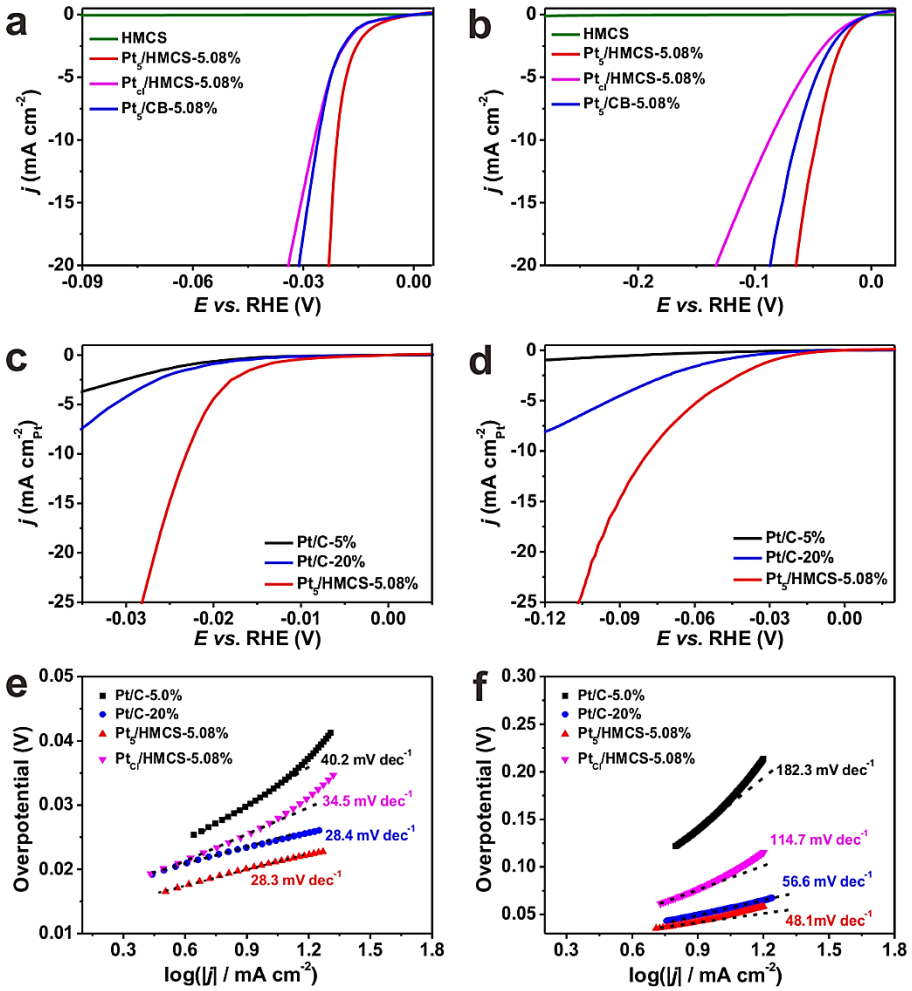

Figure 5. Electrochemical analysis of HER activity of Pt_5/HMCS. LSV curves of different catalysts in (a) 0.5 M H_2SO_4 and (b) 1.0 M KOH. LSV curves of Pt_5/HMCS (5.08 wt%) and commercial Pt/C (5 wt% and 20 wt%) catalysts based on ECSA of Pt in (c) 0.5 M H_2SO_4 and (d) 1.0 M KOH. Corresponding Tafel plots for different catalysts in (e) 0.5 M H_2SO_4 and (f) 1.0 M KOH.

for Table of Content Entry

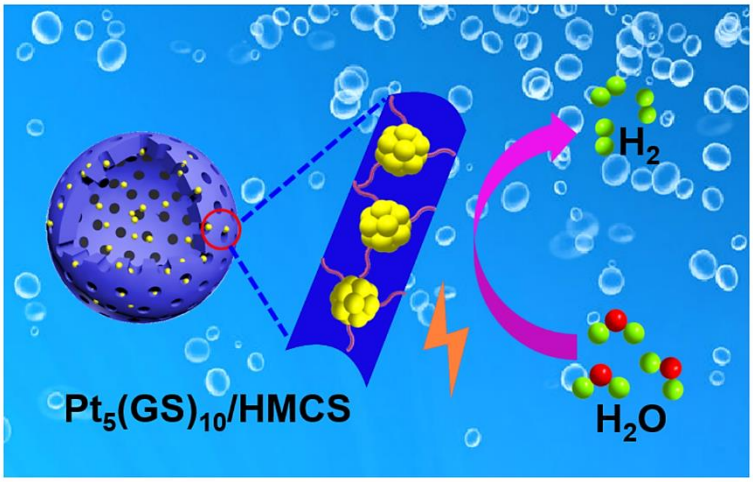

Subnanometer Pt clusters confined in mesoporous carbon nanochannels are developed as a novel electrocatalyst for hydrogen evolution reaction. The unique structure effectively stabilizes the Pt clusters during the ligand removal and catalytic process, leading to remarkable electrocatalytic performance for hydrogen production in both acidic and alkaline solutions.